Structure of electrodeposited Tl overlayers on Au(100) studied via surface X-ray scattering

J.X. Wang [a,*], R.R. Adžić [a], O.M. Magnussen [b], B.M. Ocko [b]

[a] Department of Applied Science, Chemical Sciences Division Brookhaven National Laboratory Upton, NY 11973, USA
[b] Department of Physics Brookhaven National Laboratory Upton, New York 11973, USA

Abstract

The electrodeposition of Tl on Au(100) has been investigated using surface X-ray scattering. At potentials prior to Tl bulk deposition, Tl adatoms form a c($p \times 2$) close-packed monolayer on the unreconstructed Au(100) surface in both acid and alkaline solutions. The Tl monolayer uniaxially compresses over a 0.25 V wide potential range and the nearest-neighbor-separation of Tl attains a minimum value of 3.34 Å. This is close to the value obtained on Au(111) prior to bulk Tl deposition. From the specular X-ray reflectivity, a 2.55 Å Au–Tl layer spacing is obtained for the c($p \times 2$) monolayer. Bulk deposition of Tl at potentials negative of the reversible Nernst potential results in the formation of imperfectly-aligned hexagonal-close-packed crystallites on top of the c($p \times 2$) monolayer. At potentials positive to the stripping of the c($p \times 2$) monolayer, a (2 × 2) diffraction pattern is observed in perchloric and sulfuric acid solutions but not in alkaline solutions. Real space models are proposed.

Keywords: Electrochemical methods; Epitaxy; Surface structure; Thallium; X-ray scattering

1. Introduction

The underpotential deposition (UPD) of metals has been extensively studied in the past two decades by many electrochemical and spectroscopic techniques [1–3]. These studies have shown that the crystallographic orientation of an electrode has a pronounced effect on UPD processes. In situ structural studies on surfaces with different crystallographic orientations are essential to understand how the atomic arrangement of an electrode surface influences adlayer structures and deposition processes. Since the advent of surface X-ray scattering (SXS) and scanning probe techniques, detailed in situ structural studies are possible. To date, most of these studies have been carried out on the least corrugated (111) surfaces [4–16]. Despite the strong substrate-adatom interactions, the foreign metal adlayers often form incommensurate, hexagonally close-packed monolayers at potentials slightly positive of bulk deposition. The coverages of these monolayers are mainly determined by the adatom–adatom interaction. Overall, much less is known about the structure of metal monolayers on the other two low-index faces, i.e. (100) and (110). For Ag(100) [17] and Au(100) [18], a commensurate c(2 × 2) structure is formed when Pb is deposited. In contrast, over the same potential regime on the (111) surface a close-packed incommensurate monolayer is formed. The effect of the substrate has also been demonstrated for the UPD of Cu on Au in the presence of chloride. Here, a hexagonal incommensurate structure is ob-

served on Au(111) whereas a uniaxially commensurate ($n \times 2$) structure is formed on Au(100) [19].

In this paper we report the results of an in situ SXS study of Tl electrodeposition on Au(100) in the sub-monolayer, monolayer, and multilayer coverage regimes in acid and alkaline solutions. A commensurate (2×2), a uniaxially commensurate c($p \times 2$), and an incommensurate hexagonal phase are sequentially observed with decreasing potential as the Tl coverage increases. This indicates that the effect of the substrate lattice decreases with increasing Tl coverage. A comparison of structural and voltammetric behaviors of Tl UPD on Au(100) and Au(111) are presented in order to demonstrate the role of the substrate crystallographic orientation in determining the adlayer structures.

2. Experimental aspects

The Au(100) single crystals were oriented within 0.2° of the $\langle 100 \rangle$ crystallographic plane and electrochemically polished in cyanide-containing solution. After flame annealing, the sample was transferred into an electrochemical X-ray scattering cell constructed from Kel–F [20] with a drop of water covering the surface. The cell was sealed using a 4 μm thick Prolene (Chemplex Inc.) X-ray window. The solutions were prepared from $TlNO_3$, Tl_2CO_3, (Johnson Matthey, 99.99 + %), $HClO_4$ (Merck, Suprapur), H_2SO_4 (Merck, Suprapur), NaOH (50%) solution (Fisher, 99.99 + %) and Milli-Q water (Millipore Inc.) and were kept oxygen free during the measurements. At a potential slightly positive of the bulk Tl deposition potential, the cell was deflated which leaves a thin (~ 10 μm thick) capillary electrolyte film between the Au(100) face and the X-ray window. A reversible hydrogen electrode in 0.1M $HClO_4$ or NaOH was used as a reference electrode. All potentials are cited with respect to the normal hydrogen electrode (NHE).

SXS measurements were carried out at the National Synchrotron Light Source (NSLS) at beam line X22B with $\lambda = 1.54$ Å (in-plane diffraction) and at beam line X22C with $\lambda = 1.25$ Å (X-ray specular reflectivity). A full description of the electrochemical SXS technique has been presented elsewhere [20]. For in-plane diffraction measurements,

the q-space resolution within the scattering plane was determined primarily by the Soller slits on the detector arm. This arrangement provides a 2Θ resolution of 0.1° half-width-at-half-maximum (HWHM) which corresponds to a longitudinal in-plane resolution of 0.007 Å^{-1} HWHM. The transverse in-plane resolution was limited by the mosaic spread of the gold crystal which is about 0.1° HWHM. For convenience the unit cell for Au(100) surface is chosen to have one gold atom per unit cell within the plane, i.e., with two lattice vectors pointing to in-plane nearest neighbor Au atoms (length $a = 2.884$ Å) and the third vector, c (4.078 Å), along the surface normal. A position in reciprocal space in this coordinate system is given by $(a^*, b^*, c^*) \cdot (H, K, L,)$, where $a^* = b^* = 2\pi/a = 2.178$ Å^{-1}, and $c^* = 2\pi/\sqrt{2}\,a = 1.540$ Å^{-1}. The in-plane diffraction measurements were carried out in the (H, K) plane with $L = 0.1$ corresponding to a grazing incident angle of 1.1°.

3. Results and discussion

3.1. Voltammetry

The linear potential sweep voltammetry curves for Tl UPD on Au(100) and Au(111) in 0.1M $HClO_4$ containing 5mM Tl$^+$ are shown in Fig. 1. The current spikes at -0.5 V are due to the onset of bulk deposition and dissolution which occurs close to the reversible Nernst potential of -0.472 V. The charge associated with the peaks at potentials between -0.1 and -0.3 V is 30 and 80 μC/cm^2 for Au(100) and Au(111), respectively. Assuming a one-electron exchange in the UPD of Tl, this is equivalent to only 0.15 of a monolayer for Au(100) and 0.35 for Au(111) since the monolayer coverages require 192 and 220 μC/cm^2 for these two surfaces. The actual Tl coverage in the potential region negative of the small current peaks, as determined by our SXS measurements, ranges from 0.80 to 0.85 and from 0.75 to 0.70 of a monolayer for Au(100) and Au(111) [11] surfaces, respectively. These values indicate that a sizable fraction of a Tl monolayer is deposited at more positive potentials. In fact, the current observed for Au(100) in the potential region between -0.2 and 1.1 V is larger than the double layer charging
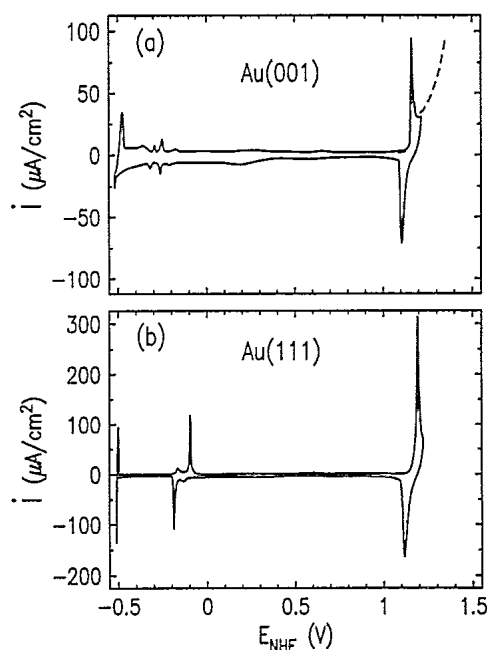
Fig. 1. Linear sweep voltammetry curves for UPD of Tl on Au(100) and Au(111) in 0.1M HClO$_4$ with 2.5mM Tl$_2$CO$_3$. Sweep rate 20 mV/s.

current for Au(100) in the absence of Tl$^+$. The large peaks around 1.1 V are associated with the surface redox Tl$^+$/Tl^{3+} reaction which can be inferred from the potential shift of the current peak which is close to 30 mV per decade change of Tl concentration. In potential scans above 1.2 V (dashed line in Fig. 1a), the bulk Tl$^+$/Tl^{3+} reaction [21], as well as the gold surface oxidation, are observed.

3.2. The c(p × 2) monolayer

Grazing incident angle X-ray diffraction measurements were carried out to determine the Tl monolayer structure in the potential region close to the bulk deposition. Fig. 2a shows the in-plane diffraction pattern observed at −0.44 V from Au(100) and the Tl monolayer in acid and alkaline solutions containing 5mM Tl$^+$. The solid circles correspond to the Au(100) substrate reflections, whereas the squares correspond to the Tl monolayer reflections in one of the two symmetry equivalent domains. The absence of the Au(100) reconstruction diffraction pattern [22] indicates that the top gold layer does not reconstruct under the Tl adlayer. The Tl diffraction pattern has a centered rectangular symmetry, i.e., all the diffrac-

tions are found at $(m\delta, n/2)$ when $m + n$ is even. The corresponding real space model is given in Fig. 2b showing the c($p \times 2$) symmetry and the quasi-hexagonal packing of Tl adatoms.

The diffracted X-ray intensity from the c($p \times 2$) Tl monolayer at $(\delta, 1/2)$, $(\delta, 3/2)$, $(2\delta, 0)$, and $(2\delta, 1)$ positions is shown in Figs. 2c and 2d. At −0.44 V, the diffraction peaks along the H direction are centered at $\delta = 0.8475$ for $K = 1/2$ and $3/2$, and $2\delta = 1.6950$ for $K = 0$ and 1. The length of the unit cell along the incommensurate direction relative to the gold spacing is given by $p = 1/\delta = 1.180$. The HWHM of the diffraction peak increases slightly as the H scan becomes closer to a radial scan at various positions since the instrumental resolution along the
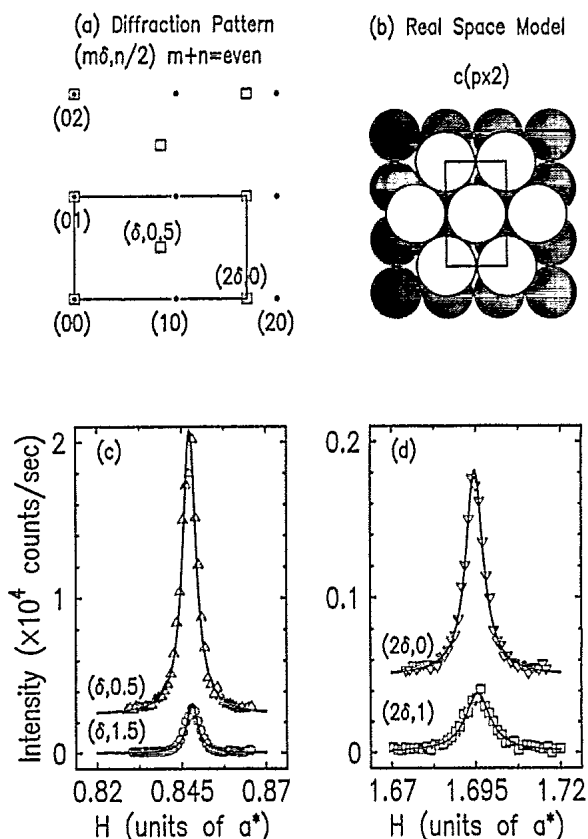

Fig. 2. (a) In-plane diffraction patterns for the c($p \times 2$) Tl monolayer (squares) on Au(100) (solid circles) obtained at −0.44 V in 0.1M HClO$_4$ with 5mM Tl$^+$. For clarity, only one of the two symmetry equivalent domains of the c($p \times 2$) phase is shown. (b) Real space model deduced from the observed diffraction pattern shown in (a). (c) and (d) Diffraction scans along the H direction through four low-order diffraction peaks of the Tl monolayer in the c($p \times 2$) phase.
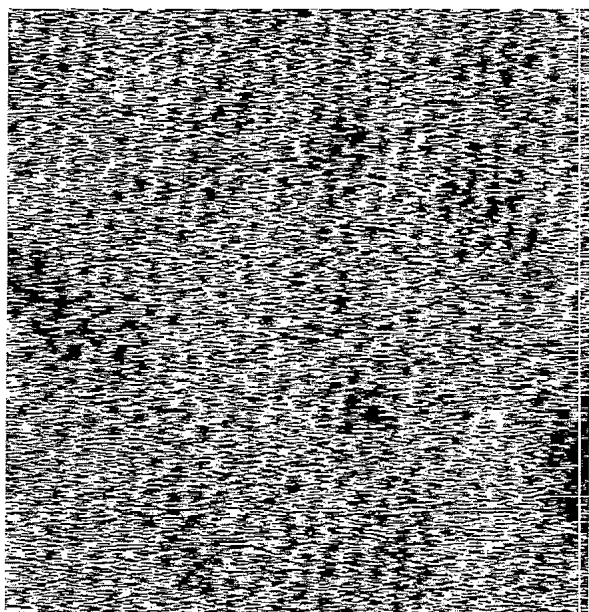
Fig. 3. In situ STM image of Au(100) in 0.1M HClO$_4$ with 5mM Tl$_2$CO$_3$ at -0.45 V (constant-current mode, unfiltered) showing a (70×70) Å^2 surface area covered by a quasi-hexagonal Tl monolayer.

the reciprocal base vector, δ. The dimensionless Tl coverage is equal to δ, which is the ratio of the Au to Tl unit cell areas. Fig. 4b shows the change of Tl coverage as a function of potential for solutions containing 5mM and 0.5mM Tl$^+$. Initially, it increases almost linearly with decreasing potential and then appears to saturate close to the bulk deposition potential.

A direct determination of adlayer coverages by in-plane diffraction measurements provides a reliable measure of the elecrosorption valence, γ, even when the total coverage change is only a few percent. The value of γ can be determined from the expression, $\gamma_{Tl} = 0.059(\partial\log(a)_s/\partial E)\Gamma_{Tl}$, where a_s is the activity of Tl$^+$ in solution [10,24]. The application of this expression to Fig. 4b, by approximating the activity with the Tl$^+$ concentration, yields $\gamma_{Tl} \sim 1$. This can also be inferred from Fig. 4b in which the 0.5mM data shifted by 0.059 V, drawn as the plus sign, overlap the 5mM data. Similar results were obtained for Tl on Au(111) [10]. Therefore, on both the (100)
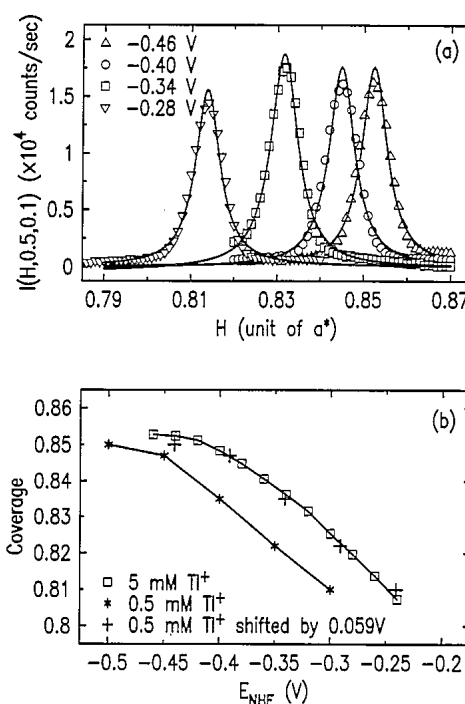
radial direction is worse than the effective transverse resolution from the sample mosaic. From the minimum HWHM, 0.0044 Å^{-1} at (δ,1.5), a lower bound on the coherence length (i.e., the domain size), 230 Å (1/0.0044 Å^{-1}), has been obtained. This value is 1/3 smaller than the Au(100) facets (380 Å). On Ag(100) the c($p \times 2$) Tl monolayer [23] has a coherence length of 200 Å with crystal facets of 300 Å. Therefore, the unreconstructed Au(100) surface seems to have large terraces free of gold clusters. In addition, we performed preliminary scanning tunneling microscopy (STM) experiments using a Nanoscope III and W-tip insulated with nailpolish. As shown in the atomic-resolution image presented in Fig. 3, an approximately hexagonal lattice with a lattice spacing of 3.3 Å was obtained at -0.45 V. This is consistent with the c($p \times 2$) structure.

In order to measure the potential dependence of the monolayer lattice parameter, p, diffraction profiles were acquired along the H direction at (δ,0.5) over the entire potential region of the c($p \times 2$) phase in increments of 0.02 V. Several representative diffraction profiles displayed in Fig. 4a, are well described by Lorentzian profiles shown as the solid lines. The peak position obtained from the fit gives

Fig. 4. (a) Diffraction intensity profiles along the H direction through the (δ,0.5) position at different potentials in 0.1M HClO$_4$ with 5mM Tl$^+$. The solid lines are the fits to a Lorentzian line shape. (b) Tl coverage calculated from the in-plane diffraction peak position as a function of potential and Tl$^+$ concentration.
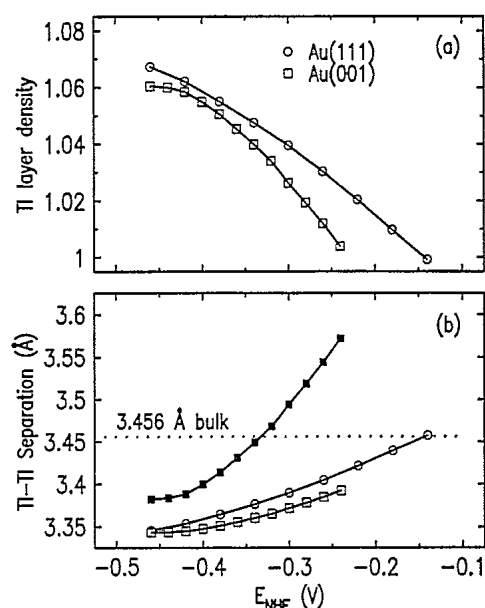
Fig. 5. (a) Tl layer density normalized to the layer density of a bulk hcp–Tl layer and (b) Tl–Tl separation as a function of potential on Au(100) and Au(111) in 0.1M HClO$_4$ with 5mM Tl$^+$. In (b) the open and filled squares are the nearest- and second-nearest-neighbor-spacings of Tl in the c(p×2) phase on Au(100), respectively; the open circles are the nearest-neighbor-spacing of Tl in the hexagonal close-packed phase on Au(111).

and (111) surfaces, Tl adatoms in the close-packed phase are fully discharged.

A detailed structural comparison between the c(p × 2) Tl monolayer on Au(100) and the rotated-hexagonal Tl monolayer on Au(111) is given in Fig. 5. The Tl layer density relative to the bulk value (1.39 × 10^{15} atoms/cm^2), calculated from the measured lattice constants, is shown in Fig. 5a for the two surfaces. On Au(111), the layer density increases in a nearly linear manner with decreasing potential, which is a common feature of a two-dimensional compressible adlayer [12,25]. For Au(100) the layer density also increases with decreasing potential, but far from a linear manner. At all the potentials, the Tl layer density is higher on Au(111) than on Au(100). These findings can be understood in terms of the distortion of the c(p × 2) lattice from the hexagonal symmetry. As shown in Fig. 5b, the separation between a Tl atom and its six surrounding neighbor atoms has one value for the hexagonal lattice on Au(111) (open circles), but two values for the c(p × 2) phase on Au(100) due to the constraint

imposed by the uniaxial commensurate nature of the phase. As visible in Fig. 2b, in the c(p × 2) phase, the Tl–Tl separation between atoms in two adjacent rows (open squares) is smaller than the separation of Tl adatoms in the same row (filled squares). The former is close to the Tl–Tl separation on the Au(111) surface over the whole potential range of the c(p × 2) phase and reaches precisely the same value at the negative potential end. This suggests that the lower layer density on Au(100) results from the decrease of packing efficiency due to the symmetry distortion rather than the change of adatom–adatom interaction. At the positive potential end, the c(p × 2) and the hexagonal phases vanish at slightly different potentials, but their minimum layer density is essentially the same.

In order to determine the adlayer structure along the surface normal direction and to check for any surface inhomogeneity which may result from the Au(100) reconstruction or Tl–Au alloy formation, specular X-ray reflectivity measurements were carried out. Fig. 6 shows the absolute reflectivity obtained at −0.45 V by integrating rocking curves at each L and normalizing to the direct beam as described in detail elsewhere [26]. The data deviate from the calculated reflectivity profile for the ideally
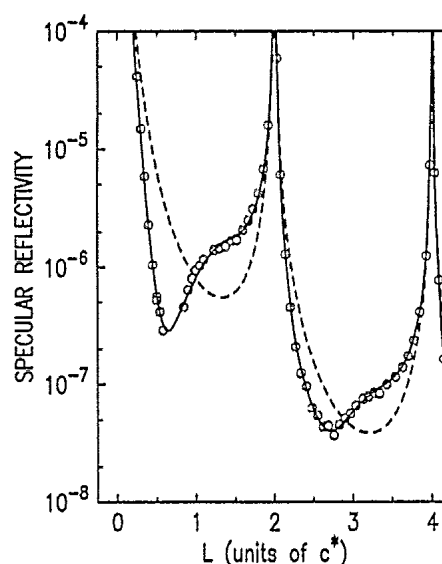

Fig. 6. X-ray specular reflectivity (circles) from the c(p×2) Tl monolayer on Au(100) at −0.45 V. The dashed line is calculated for an ideally terminated Au(100) crystal. The fitted reflectivity from the model discussed in the text is shown by the solid line.

Table 1
Parameters obtained from analysis of specular reflectivity data

Atom	Coverage	Spacing (Å)	rms (Å)
Au	1.00 ± 0.02	2.13 ± 0.04	0.13 ± 0.02
Tl	0.86 ± 0.04	2.55 ± 0.04	0.38 ± 0.04
Tl	0.18 ± 0.04	3.64 ± 0.14	0.59 ± 0.14

terminated Au(100) crystal at intermediate wave vectors between the Bragg peaks at L equal to 2 and 4. The best fit of the data is obtained by using a three-surface-layer model with the parameters listed in Table 1. These layers correspond to the gold top layer, the Tl monolayer, and another nominal Tl adlayer which contains the adsorbed Tl^+ ions and water molecules. The electron density profile for each layer is described by three parameters (density, spacing, and root-mean-square (rms) atomic displacement). The surface enhancement and absorption corrections have been incorporated in the analysis. The top gold layer has the same density and slightly increased layer spacing as the bulk gold layers. The Tl coverage in the $c(p \times 2)$ phase is 0.86 which is consistent with the coverage (0.852) calculated from the in-plate lattice parameters. These results suggest that there is no extensive surface alloy at this potential. The Au–Tl layer spacing of 2.55 Å is smaller than 2.66 Å measured for Au(111). This is expected assuming that all the Tl adatoms are between the gold rows in the $c(p \times 2)$ phase on Au(100). The small electron density in the layer on top of the $c(p \times 2)$ monolayer might result from weakly bonded Tl^+ ions and/or water molecules. For this layer the layer spacing and rms values are much greater than in the $c(p \times 2)$ Tl monolayer.

3.3. Bulk Tl deposit on the c(p × 2) monolayer

X-ray diffraction measurements were carried out at −0.52 V, 50 mV negative of the Nernst potential for Tl bulk deposition, in order to explore the initial phases of bulk Tl deposition. The bulk Tl deposit was grown by keeping the cell inflated until at least 30 equivalent monolayers of Tl (estimated from the observed cathodic current) were deposited on the crystal surface. After the cell was deflated, further

deposition on the sample surface was limited by the depletion of Tl^+ in the remaining thin layer of solution. Despite the bulk deposition, the diffraction from the $c(p \times 2)$ Tl monolayer did not shift in position or change in intensity. Additional diffraction peaks which exhibit hexagonal symmetry appear. The peak widths are 2 to 3 times wider than that from the $c(p \times 2)$ monolayer. The hexagonal lattice constant calculated from the peak position (3.44 Å) is close to the bulk hexagonal lattice constant (3.456 Å) obtained in the close-packed-hexagonal (hcp) phase.

The hexagonal diffraction pattern is attributed to the ordered bulk Tl formed on top of the first $c(p \times 2)$ Tl adlayer. This is verified by the L dependence of the in-plane peaks. The intensity from the $c(p \times 2)$ phase at (0.852,0.5) decreases monotonically with increasing L from 0.1 to 2. This dependence is expected for a two-dimensional monolayer which has no periodic structure along the surface normal direction. On the other hand, the scattered intensity at the hexagonal in-plane position (0.840,0.491) exhibits a sharp peak at $L = 0.72$, which is a convincing signature of a three-dimensional crystal. The calculated Tl layer spacing is 2.83 Å, which is close to the expected value of 2.80 Å found for hcp bulk Tl.

Detailed diffraction features vary slightly with different deposition potentials which gives a 0.03 Å uncertainty in both in-plane and surface normal lattice constants and a 0.4° range of the rotation angles from the substrate axes. These facts suggest that imperfectly-aligned hcp crystallites are formed on top the $c(p \times 2)$ monolayer. Previous SXS study of Pb overpotential deposition on Ag(111) [5] showed that the hexagonal monolayer, which is compressed 2.8% relative to bulk Pb–Pb nearest-neighbor separation, restructs after the deposition of approximately five equivalent monolayers of Pb and the deposition of more than 100 equivalent monolayers results in islands that have (111) texture of fcc Pb but are randomly oriented in the plane of the substrate. The failure of lead to grow epitaxially was attributed to the large compressive strain of the Pb monolayer. Although the compression of the $c(p \times 2)$ Tl monolayer is similar to Pb on Ag(111), the monolayer stability and the structure of bulk deposits are different in the two cases. Further studies have been
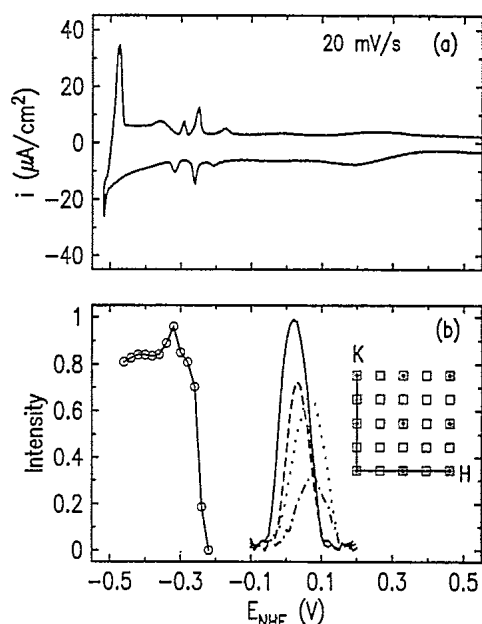
Fig. 7. Current–potential curve (adapted from Fig. 1) (a) and X-ray diffraction intensities from the c(p×2) and the (2×2) phases (b) for UPD of Tl on Au(100) in 0.1M HClO₄ with 5mM Tl⁺. The circles are the integrated intensity for the (δ,0.5) peak of the c(p×2) phase. The solid (dotted) and dashed (dashed-dotted) lines are the peak intensity at (0,0.5) and (0.5,0.5) while the potential was decreased (increased) at a rate of 0.33 mV/s, respectively. The inset in (b) shows the in-plane diffraction pattern of the (2×2) phase (squares) on Au(100) (solid circles).

carried out on Ag(100) and detailed discussions of the roles of the monolayer structure and substrate–overlayer interactions will be presented elsewhere [27].

3.4. The (2 × 2) monolayer

We now turn our attention to the potentials positive of the c(p × 2) phase region. In particular, we will discuss an ordered (2 × 2) phase which is observed between −0.05 and 0.15 V. In Fig. 7, the voltammetry curve is plotted along with the potential dependent scattered intensity in the c(p × 2) phase and at the (0,0.5) and (0.5,0.5) positions on the same potential scale. The integrated intensity associated with the c(p × 2) phase (circles) starts to decrease above −0.3 V and vanishes by −0.22 V. This phase transition potential region is well correlated with the current peak at −0.25 V shown in the voltammetry

curve. As discussed in Section 3.1, the charge associated with the current peak at −0.25 V is very small in comparison to the Tl coverage before the phase transition. Thus, a considerable amount of Tl remains adsorbed and may undergo another structural transition at potentials above −0.25 V. In order to determine whether a commensurate c(2 × 2) or (2 × 2) phase forms at potentials positive to −0.25 V, the scattered intensities at (0,0.5) and (0.5,0.5) were measured during potential sweeps. As shown in Fig. 7b, the scattered intensity at these two positions exhibits a peak around 0.03 V with a small hysteresis between the two sweep directions indicating the presence of an ordered phase in the potential region. Between −0.25 and −0.05 V, no diffraction features from an ordered Tl phase were observed.

The measurements at 0.03 V revealed diffractions at (m/2,n/2) with m and n up to 4 as shown in the inset in Fig. 7b. Since a c(2 × 2) structure only gives rise to the diffractions at (m/2,n/2) with the sum of m and n being an even number, the observation of all the half-order diffractions is indicative of a primary (2 × 2) unit cell. Four low-order peaks are shown in Fig. 8a. The coherence length calculated from the minimum peak width at (0.5,1.5) is 210 Å which is similar to that of the c(p × 2) phase. The scattered intensity at (0.5,1) decreases monotonically with L, which is characteristic for a single layer. The integrated intensities for both the c(p × 2) and the (2 × 2) structures were calculated from the intensities along the H direction and the peak widths along the K direction. The intensity ratio for the c(p × 2) and the (2 × 2) phases is found to be 6.0 ± 0.3 which is very close to the value of 5.8 ((0.85/0.25)²/2) expected from the electron density ratio by assuming the Tl coverage is 0.85 and 0.25, in the c(p × 2) and (2 × 2) phases, respectively. The divisor of 2 accounts for the two symmetry domains in the c(p × 2) phase. Based on these observations, three real space models for the (2×2) phase are proposed.

The simplest model (top panel of Fig. 8b) is a primitive (2 × 2) structure with four Tl adatoms at the corners of the 2 × 2 square unit cell and a Tl coverage of 1/4. This model can be rationalized in terms of adsorption of partially-charged (hence a large separation) Tl adatoms on the hollow sites of Au(100) within a suitable potential region. The an-
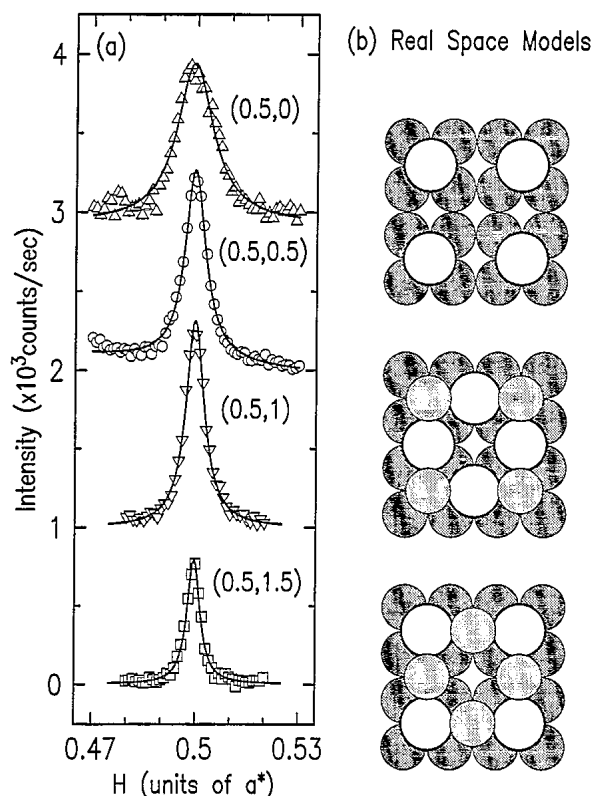
Fig. 8. (a) Diffraction scans along the H direction through four low-order diffractions of the (2×2) phase at 0.03 V in 0.1M $HClO_4$ with 5mM Tl^+. The solid lines are the fits to the Lorentzian line shape. (b) Real space models with (2×2) unit cell. The open circles represent Tl adatoms, the light-shaded circles represent the Au atoms within the Tl adlayer, and the dark-shaded circles represent the underlying Au(100) surface.

odic charge measured from −0.22 to 0.03 V in the voltammetry curve is, however, only half of the charge required for dissolution of 0.55 (0.8 − 0.25) monolayers of Tl. Thus, this simple model appears unlikely, but can not be completely ruled out. In addition, potential step experiments show that the formation of the (2 × 2) phase exhibits slow kinetics on a time scale of 2 to 20 min. Hence, the charge measured from the voltammetry curve (at 20 mV/s sweep rate) might be less than the total dissolution charge.

Preliminary in situ STM experiments show changes in the gold substrate morphology at potentials above −0.2 V that suggest the formation of a mixed Tl/Au−surface layer [23]. We therefore pro-

pose two other models which involve Au atoms. These models are also consistent with the SXS data, since the calculated scattering intensities from models with coverages of 1/4 and 3/4 in the (2 × 2) phase are the same at all the half-order positions if we ignore the small form-factor difference between Au and Tl. The two models having either 2/4 Tl and 1/4 Au or 1/4 Tl and 2/4 Au monolayers are shown in the middle and bottom panels of Fig. 8b. The formation of such a mixed layer is likely to exhibit kinetics behavior which is slower than a single component adlayer.

Since the coadsorption of anions is possible in this potential region, the anions were varied in the thallium salts and the supporting electrolytes. The same diffraction pattern and similar phase behavior were observed in the following three solutions: $TlNO_3$ or Tl_2CO_3 in 0.1M $HClO_4$ and $TlNO_3$ in 0.05 H_2SO_4. The addition of 5mM NaCl into the solution shifts the potential region of the (2 × 2) phase by about −80 mV. Although the (2 × 2) phase is not anion sensitive in acid solutions, it does not appear in 0.1M NaOH electrolyte. Further studies with other techniques are needed to identify the real components for this (2 × 2) phase.

4. Conclusions

The SXS study of Tl UPD on Au(100) reveals the formation of a close-packed c(p × 2) Tl monolayer prior to the bulk deposition which uniaxially compresses with decreasing potential over a 0.25 V wide potential range. As on Au(111), the nearest-neighbor-separation of Tl in the monolayer reaches the minimum value of 3.34 Å before bulk deposition. Bulk deposition of Tl at potentials negative of the reversible Nernst potential results in the formation of imperfectly-aligned hcp crystallites on top of the c(p × 2) monolayer. After stripping the c(p × 2) monolayer at positive potentials, a (2 × 2) diffraction pattern was observed at potentials between −0.05 and 0.15 V in perchloric and sulfuric acids but not in alkaline solutions. The real space models consistent with the observed (2 × 2) diffraction feature are proposed. A determination of the components within the (2 × 2) unit cell, as well as the phase behavior of

Tl at potentials positive of −0.2 V, requires further study.

Acknowledgements

References

[1] D.M. Kolb, in: Advances in Electrochemistry and Electrochemical Engineering, Vol. 11, Eds. H. Gerischer and C.W. Tobias (Wiley-Interscience, New York, 1978) pp. 125–271.

[2] R.R. Adzic, in: Advances in Electrochemistry and Electrochemical Engineering, Vol. 13, Eds. H. Gerischer and C.W. Tobias (Wiley-Interscience, New York, 1984) pp. 159–260.

[3] P.N. Ross, in: Structure of Electrified Interfaces, Eds. J. Lipkowski and P.N. Ross (VCH, New York, 1993) pp. 35–64.

[4] (a) M.G. Samant, M.F. Toney, G.L. Borges, L. Blum and O.R. Melroy, Surf. Sci. 193 (1988) L29. (b) O.R. Melroy, M.F. Toney, G.L. Borges, M.G. Samant, J.B. Kortright, P.N. Ross and L. Blum, Phys. Rev. B 38 (1988) 10962.

[5] O.R. Melroy, M.F. Toney, G.L. Borges, M.G. Samant, J.B. Kortright, P.N. Ross and L. Blum, J. Electroanal. Chem. 258 (1989) 403.

[6] M.F. Toney, J.G. Gordon, M.G. Samant, G.L. Borges, D.G. Wiesler, D. Yee and L.B. Sorensen, Langmuir 7 (1991) 796.

[7] (a) M.F. Toney, J.G. Gordon, G.L. Borges, O.R. Melroy, M.G. Samant, D. Wiesler, D. Yee and L.B. Sorensen, Phys. Rev. B 42 (1990) 5594. (b) M.F. Toney, J.G. Gordon, M.G. Samant, G.L. Bordes, O.R. Melroy, D. Yee and L.B. Sorensen, Phys. Rev. B 45 (1992) 9362.

[8] C.-H. Chen, K.D. Keple, A.A. Gewirth, B.M. Ocko and J. Wang, J. Phys. Chem. 97 (1993) 7290.

[9] R.R. Adzic, J. Wang, C.M. Vitus and B.M. Ocko, Surf. Sci. 293 (1993) 876.

[10] J.X. Wang, R.R. Adzic and B.M. Ocko, J. Phys. Chem. 98 (1994) 7182.

[11] R.R. Adzic, J.X. Wang, W. Polewska and B.M. Ocko, Electrochim. Acta 40 (1995) 83.

[12] M.F. Toney, J.G. Gordon, M.G. Samant, G.L. Borges, O.R. Melroy, D. Yee and L.B. Sorensen, J. Phys. Chem. 99 (1995) 4733.

[13] (a) O.M. Magnussen, J. Hotlos, G. Beitel, D.M. Kolb and R.J. Behm, J. Vac. Sci. Technol. B 9 (1991) 969. (b) O.M. Magnussen, J. Hotlos, R.J. Nichols, D.M. Kolb and R.J. Behm, Phys. Rev. Lett. 64 (1990) 2929. (c) S. Manne, P.K. Hansma, J. Massie, V.B. Elings and A.A. Gewirth, Science 251 (1991) 183.

[14] C.-H. Chen and A.A. Gewirth, J. Am. Chem. Soc. 114 (1992) 5439.

[15] (a) C.-H. Chen, S.M. Vesecky and A.A. Gewirth, J. Am. Chem. Soc. 114 (1992) 451. (b) C.-H. Chen and A.A. Gewirth, Phys. Rev. Lett. 68 (1992) 1571.

[16] W. Polewska, J.X. Wang, B.M. Ocko and R.R. Adzic, J. Electrocanal. Chem. 376 (1994) 41.

[17] W. Obretenov, U. Schmidt, W.J. Lorentz, G. Staikov, E. Budevski, D. Carnal, U. Muller, H. Siegenthaler and E. Schmidt, J. Electrochem. Soc. 140 (1992) 692.

[18] K.M. Robinson and W.E. O'Grady, in: Synchrotron Techniques in Interfacial Electrochemistry, Vol. 432, Eds. C.A. Melendres and A. Tadjeddine (Kluwer, Boston, 1994) pp. 157–169.

[19] F. Moller, O.M. Magnussen and R.J. Behm, Phys. Rev. B 51 (1995) 2484.

[20] J. Wang, B.M. Ocko, A.J. Davenport and H.S. Isaacs, Phys. Rev. B 46 (1992) 10321.

[21] M. Pourbaix, in: Atlas of Electrochemical Equilibria in Aqueous Solutions (NACE, Cebelcor, 1960) p. 445.

[22] B.M. Ocko, J. Wang, A.J. Davenport and H.S. Isaacs, Phys. Rev. Lett. 65 (1990) 1466.

[23] Unpublished results.

[24] J.W. Schultze and K.J. Vetter, J. Electroanal. Chem. 64 (1973) 63.

[25] (a) B.M. Ocko, G.M. Gavin and J. Wang, J. Phys. Chem. 98 (1994) 897. (b) O.M. Magnussen, B.M. Ocko, R.R. Adzic and J.X. Wang, Phys. Rev. B 51 (1995) 5510.

[26] B.M. Ocko and J. Wang, in: Synchrotron Techniques in Interfacial Electrochemistry, Vol. 432, Eds. C.A. Melendres and A. Tadjeddine (Kluwer, Boston, 1994) pp. 127–155.

[27] J.X. Wang, R.R. Adzic, O.M. Magnussen and B.M. Ocko, Surf. Sci., submitted.